

PAPER

Linear and nonlinear ultrasound fields formed by planar sources with random pressure distributions

Tomoo Kamakura*, Hideyuki Nomura† and Gregory T. Clement‡

The University of Electro-Communications, 1-5-1, Chofugaoka, Chofu, 182-8585 Japan

(Received 16 September 2014, Accepted for publication 8 December 2014)

Abstract: The goal of the present study is to clarify the formation and behavior of sound pressure fields from a statistical point of view when the individual transducers constituting an array source have random performances or, alternatively, conversion efficiencies from electric to acoustic power that vary with the individual transducer. Linear and nonlinear fields are considered herein. Based on experimental data, we assume that the amplitudes and phases of pressure signals emitted from the transducers are random variables that obey Gaussian distributions. The phase changes are, however, not taken into consideration in our theory subject to their small effects on the field formation. Spatial variation in pressure fields attributed to the random performance of transducers is large near the source, and fades with propagation in the farfield. Linear theory predicts that the mean value of the pressure amplitudes is the same as the value when the pressure on the array source is distributed uniformly. Interestingly, the standard deviation around the mean pressure is independent of the radial distance in the plane perpendicular to the beam axis, being inversely proportional to the square root of the number of transducers. For the second-harmonic components, both the mean value and standard deviation are dependent on the radial distance. The validity of these theoretical findings is verified by Monte Carlo simulation and experimental data.

Keywords: Random distribution, Ultrasonic beam, Nonlinear propagation, Monte Carlo simulation

PACS number: 43.25.Cb, 43.28.Lv [doi:10.1250/ast.36.208]

1. INTRODUCTION

Ultrasonic fields formed by a finite aperture source are generally complicated due to diffraction, especially in the nearfield. Even so, we can, in principle, theoretically predict such fields using the wave equation associated with the appropriate boundary conditions. This approach is extended to an arbitrary array source that usually consists of many transducers. Generally, the electro-acoustic performance of piezoelectric ultrasonic transducers, or, alternatively, their conversion efficiencies from electric to acoustic power, differ individually even when the transducers are produced under controlled environments. Even in such a situation, if the individual transducer is identified with respect to its performance, sound fields from the array source should be precisely predicted by wave theories pertinent to our concern. However, measuring the individual performances of a large number of transducers is a laborious task.

To date, the effects of variation in the design parameters of an ultrasonic transducer, such as capacitance and resonant frequency, on its performance characteristics have been extensively investigated. For example, Kwun *et al.* calculated the transducer performance based on the transmission line model of Krimholtz, Leedom, and Matthaei [1]. They showed that, in general, the resonant frequency and four other major parameters of a piezoelectric transducer have crucial effects on its performance. Unfortunately, they do not mention the relationship between variability in design parameters and the sound fields formed by the transducer. Wooh and Shi elaborated on the influence of the transducer's dimensions in linear phased arrays on beam steering behaviors for determining optimal transducer design parameters [2]. Their design objectives were to minimize the main-lobe width, to squelch grating lobes, and to suppress the side-lobe amplitudes. Later, the group of Wooh extended their analysis to the oversized array transducers to eliminate grating lobes as a direct consequence of the transducer shape [3]. Interestingly, ultrasonic phased arrays consisting of transducers larger than one wavelength have been developed using the concept of sparse random placement

*e-mail: kamakura@uec.ac.jp

†e-mail: h.nomura@uec.ac.jp

‡e-mail: gclement@physics.org

of the transducers for tissue ablation applications in the medical field [4,5].

Being different from the previous reports mentioned above, the present research is motivated by a statistical approach to characteristic evaluation of ultrasonic fields. In particular, our interest is to obtain information about the statistical relevance between transducer performance and their respective sound fields in order to aid in the design of an array source. Our curiosity is not limited to analysis in linear fields, i.e., we also investigate the statistical relevance in nonlinear fields. In fact, a sound beam of finite amplitude distorts its waveform during propagation due to the inherent nonlinearity of the medium. Since this nonlinear process produces harmonic distortion, the variation in performance of transducers should affect the formation of not only linear but nonlinear sound fields. In order to evaluate the effects of these variations on field formation, we consider the behaviors of statistic quantities such as the mean value of sound pressure amplitudes, based on experimental evidence indicating that the statistical quantities related to performance obey Gaussian distributions.

The remainder of the present study is devoted to examination of the statistical relationship between the transducer performance and pressure field in terms of the mean value and standard deviation. First, theoretical analysis is focused on linear fields. Next, this approach is extended to the case of second-harmonic pressure fields under weak nonlinearity. Finally, in order to verify the validity of the theoretical findings, computer simulations are executed using the Monte Carlo method. Moreover, statistical estimators for field characteristics are compared with previously reported experimental data [6].

2. STATISTICAL APPROACH

To begin with, let us assume a theoretical model of the ultrasonic source whose aperture is planar and whose typical dimension is much larger than the wavelength. We also assume that ultrasonic waves radiated from the source propagate along the z -axis or the beam axis in free space. The coordinate variables in the plane perpendicular to the z -axis are x and y in the radial direction.

Incidentally, an ultrasonic beam of finite amplitude distorts its waveform during propagation. In this situation, harmonics or combination frequency components other than the original spectral components newly appear in the distorted wave. In order to theoretically predict such spectral components, we often use the Khokhlov-Zabolotskaya-Kuznetsov (KZK) parabolic equation [7]:

$$\nabla_{\perp}^2 p - \frac{2}{c_0} \frac{\partial^2 p}{\partial z \partial t'} + \frac{b'}{\rho_0 c_0^4} \frac{\partial^3 p}{\partial t'^3} = -\frac{\beta}{\rho_0 c_0^4} \frac{\partial^2 p^2}{\partial t'^2}, \quad (1)$$

where ∇_{\perp}^2 is the two-dimensional Laplacian containing the variables x and y , p is the sound pressure, c_0 is the speed of

sound at small amplitude, $t' = t - z/c_0$ is the retarded time, b' is a coefficient related to sound absorption, and β and ρ_0 are the nonlinearity coefficient and density of a medium, respectively.

When nonlinearity is weak, Eq. (1) can be solved analytically using the method of successive approximation. Thus, the fundamental pressure p_1 and second harmonic pressure p_2 satisfy the following equations, respectively:

$$\nabla_{\perp}^2 p_1 - \frac{2}{c_0} \frac{\partial^2 p_1}{\partial z \partial t'} = 0, \quad (2)$$

$$\nabla_{\perp}^2 p_2 - \frac{2}{c_0} \frac{\partial^2 p_2}{\partial z \partial t'} = -\frac{\beta}{\rho_0 c_0^4} \frac{\partial^2 p_1^2}{\partial t'^2}. \quad (3)$$

The sound absorption term that corresponds to the third term of the left-hand side of Eq. (1) is discarded here for simplicity.

2.1. Fundamental Components

We assume that an ultrasonic source radiates monochromatic waves of angular frequency ω . By substituting $p_1 = \text{Im}[q_1 e^{j\omega t'}]$ into Eq. (2), where the notation $\text{Im}[c]$ denotes the imaginary part of a complex number c , we obtain the following equation for the complex pressure q_1 :

$$\nabla_{\perp}^2 q_1 - j2k \frac{\partial q_1}{\partial z} = 0. \quad (4)$$

The solution of Eq. (4) is written as [8]

$$q_1 = j \frac{k}{2\pi z} \int_{-\infty}^{\infty} \int_{-\infty}^{\infty} q_0(x', y') \times \exp\left[-j \frac{k}{2} \frac{(x-x')^2 + (y-y')^2}{z}\right] dx' dy', \quad (5)$$

where $k = \omega/c_0$ is the wavenumber, $q_0(x', y')$ denotes the pressure distribution function on the source face or aperture, and the double integration is performed over the face element $dx' dy'$.

Now, let us consider the case in which the source is composed of a number of small transducers. When the area of the source face is S and the number of transducers is N , the area of the transducer aperture is given by S/N if the transducers are of identical size and are allocated densely over the face. Thus, Eq. (5) is approximated by replacing the integral with summation:

$$q_1 = j \frac{k}{2\pi z} \frac{S}{N} \sum_{n=1}^N q_0(n) \exp\left[-j \frac{k}{2} \frac{(x-x_n)^2 + (y-y_n)^2}{z}\right], \quad (6)$$

where $q_0(n)$ is the representative pressure amplitude generated by only the n th transducer, although in reality it will, to some extent, depend on any other surrounding transducers through mutual acoustic coupling [9]. The variables (x_n, y_n) in Eq. (6) are the representative x and y

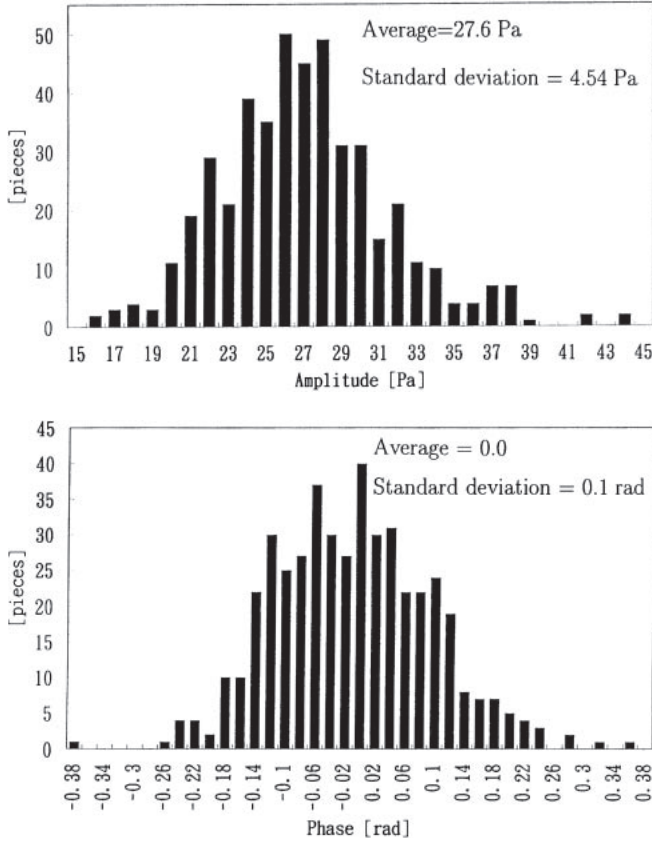


Fig. 1 Variations of the received pressure amplitudes (above) and phases (below) experimentally obtained from 456 small piezoelectric ceramic transducers. The input voltage applied to each transducer is $6V_{p-p}$ and the driving frequency is 30 kHz. The separation distance between the transducer and a 1/4-inch condenser microphone is 1 cm [10].

coordinates, for example, the center position of the n th transducer.

Even if transducers are produced under controlled environments, their electro-acoustic conversion efficiencies vary from transducer to transducer. Figure 1 shows the measured pressure amplitudes and phases of sound waves for 456 airborne piezoelectric ceramic transducers that were commercially available. The transducers individually driven at a frequency of 30 kHz and a voltage of $6V_{p-p}$ [10]. Moreover, all of the transducers have the same aperture diameter of 1 cm. A 1/4-inch condenser microphone is used to measure the sound pressure emitted from the transducer. The distance between the transducer and the microphone is 1 cm.

Both the pressure amplitudes and phases are apparently scattered within limited ranges. In addition, the distribution curves appear to be Gaussian functions. Based on the assumption that they obey the Gaussian functions, the mean value and standard deviation of the pressure amplitudes were determined to be 27.6 Pa and 4.54 Pa, respectively. Those of the phases were 0 and 0.1 radians,

where the phase data are shifted so that the mean value is 0. Intrinsically, the amplitude and phase must be correlated with each other. The correlation coefficient was measured to be 0.63. The present report, however, does not consider such correlation because the standard deviation of the phases is not expected to significantly affect the field formation. (Appendix A) Hereafter, we examine sound pressure fields by neglecting the variance of the phases for simple analysis.

Based on the above assumptions, we now consider a statistical problem regarding the mean value of the sound pressure q_1 . By taking the ensemble average of Eq. (6), we obtain

$$\langle q_1 \rangle = \frac{jk}{2\pi z} \frac{S}{N} \sum_{n=1}^N \langle q_0(n) \rangle \exp \left[-j \frac{k}{2} \frac{(x-x_n)^2 + (y-y_n)^2}{z} \right], \quad (7)$$

because $q_0(n)$ becomes a random variable of the source pressure amplitude. By setting the average $\langle q_0(n) \rangle$ with the mean pressure P_0 , we obtain

$$\langle q_1 \rangle = \frac{jk}{2\pi z} \frac{SP_0}{N} \sum_{n=1}^N \exp \left[-j \frac{k}{2} \frac{(x-x_n)^2 + (y-y_n)^2}{z} \right]. \quad (8)$$

Note that the mean pressure $\langle q_1 \rangle$ is the same as the pressure when the source pressure amplitude is uniformly distributed over the aperture with P_0 .

Next, we consider the variance σ_1^2 of the pressure amplitude, which is calculated as the expected value of the squared deviation from the mean. Since the deviation is given by $\Delta q_1 = q_1 - \langle q_1 \rangle$, it follows for the variance that

$$\begin{aligned} \sigma_1^2 &= \langle \Delta q_1 \Delta q_1^* \rangle \\ &= \left(\frac{kS}{2\pi z N} \right)^2 \sum_{n=1}^N \sum_{m=1}^N \langle \Delta q_0(n) \Delta q_0^*(m) \rangle \\ &\quad \times \exp \left[-j \frac{k}{2} \frac{(x-x_n)^2 + (y-y_n)^2}{z} \right] \\ &\quad \times \exp \left[j \frac{k}{2} \frac{(x-x_m)^2 + (y-y_m)^2}{z} \right], \quad (9) \end{aligned}$$

where $\Delta q_0(n) = q_0(n) - P_0$, and $*$ indicates the complex conjugate. All transducers are assumed to have a common covariance σ^2 and be statistically independent of each other, i.e.,

$$\langle \Delta q_0(n) \Delta q_0^*(m) \rangle = \sigma^2 \delta_{nm}, \quad (10)$$

where δ_{nm} is the Kronecker delta. Then, Eq. (9) is written as

$$\sigma_1^2 = \left(\frac{kS}{2\pi z N} \right)^2 \sigma^2 N = \left(\frac{kS}{2\pi z} \right)^2 \frac{\sigma^2}{N}. \quad (11)$$

The standard deviation given by the square root of the variance yields

$$\sigma_1 = \frac{kS}{2\pi z} \frac{\sigma}{\sqrt{N}}. \quad (12)$$

In other words, the standard deviation σ_1 of the pressure field in the linear field is directly proportional to that of the transducer performance σ . In addition, σ_1 decreases in inverse proportion to z , the distance between the source and receiving point, and the square root of the number of transducers N . Accordingly, we expect the variation σ_1 to decrease as N increases. This result is statistically the same as a sample mean having a variance that is inversely proportional to the number of samples when the samples are uncorrelated [11]. Note also that σ_1 is dependent on only the variable z and is independent of the variables x and y . In contrast, if the transducers are highly correlated, the relation $\langle \Delta q_0(n) \Delta q_0^*(m) \rangle = N\sigma^2 \delta_{nm}$ is obtained [11]. In this case, Eq. (12) takes a different form

$$\sigma_1 = \frac{kS}{2\pi z} \sigma, \quad (13)$$

and is independent of N . Practically speaking, the transducers are somewhat correlated due to mutual coupling, so that Eq. (12) may well be only a lower bound to the expected deviation, for the same reason as the stochastic process of uncorrelated random samples [11].

In the farfield, the magnitude of the pressure $\langle q_1 \rangle$ in Eq. (8) can be approximated as

$$|\langle q_1 \rangle| \simeq \frac{kS}{2\pi N} \frac{N}{z} P_0 = \frac{kS}{2\pi z} P_0 \quad (\text{on the beam axis}). \quad (14)$$

From Eqs. (12) and (14), the coefficient of variation (CV), which is defined as the ratio of the standard deviation to the mean value takes the following form in the farfield:

$$CV_1 = \frac{\sigma_1}{|\langle q_1 \rangle|} = \frac{\sigma}{P_0} \frac{1}{\sqrt{N}}. \quad (15)$$

Thus, CV_1 in the pressure field is directly related to the CV of transducers σ/P_0 . In the same fashion as the standard deviation, CV_1 is inversely proportional to the square root of N . This means that even if CV is large, the field CV_1 becomes small when the number of transducers is large.

2.2. Second-harmonic Components

Using the relationship between the second-harmonic sound pressure p_2 and its complex pressure q_2 , this is $p_2 = \text{Im}[q_2 e^{j2\omega t}]$, and Eq. (3) is reformed as

$$\nabla_{\perp}^2 q_2 - j4k \frac{\partial q_2}{\partial z} = -j \frac{2\beta k^2}{\rho_0 c_0^2} q_1^2. \quad (16)$$

In order to derive the mean value of q_2 , we take the ensemble average for both sides of Eq. (16):

$$\nabla_{\perp}^2 \langle q_2 \rangle - j4k \frac{\partial \langle q_2 \rangle}{\partial z} = -j \frac{2\beta k^2}{\rho_0 c_0^2} \langle q_1^2 \rangle. \quad (17)$$

Using Eq. (6) for the term $\langle q_1^2 \rangle$, it follows that

$$\langle q_1^2 \rangle = \left(j \frac{kS}{2\pi z N} \right)^2 \sum_{n=1}^N \sum_{m=1}^N \langle q_0(n) q_0(m) \rangle \exp \left[-j \frac{k}{2} \frac{(x-x_n)^2 + (y-y_n)^2 + (x-x_m)^2 + (y-y_m)^2}{z} \right]. \quad (18)$$

Since the source pressure $q_0(n)$ is real, the relation $\langle q_0(n) q_0(m) \rangle = P_0^2 + \sigma^2 \delta_{nm}$ holds. Roughly, $\langle q_0(n) q_0(m) \rangle \simeq P_0^2$ because of $P_0^2 \gg \sigma^2$. Hence, the mean value of the second-harmonic component $\langle q_2 \rangle$ satisfies the following equation:

$$\begin{aligned} \nabla_{\perp}^2 \langle q_2 \rangle - j4k \frac{\partial \langle q_2 \rangle}{\partial z} &= -j \frac{2\beta k^2}{\rho_0 c_0^2} \langle q_1^2 \rangle \\ &\simeq -j \frac{2\beta k^2}{\rho_0 c_0^2} \langle q_1 \rangle^2. \end{aligned} \quad (19)$$

From this equation, we note that the mean of the second-harmonic agrees approximately with the value of when the source is excited by a uniform distribution with P_0 over the face.

Finally, let us focus on the variance of the second harmonic pressure. To this end, we write the deviation as $\Delta q_2 = q_2 - \langle q_2 \rangle$. Subtracting Eqs. (17) from Eq. (16) yields

$$\nabla_{\perp}^2 \Delta q_2 - j4k \frac{\partial \Delta q_2}{\partial z} = -j \frac{2\beta k^2}{\rho_0 c_0^2} Q. \quad (20)$$

Here, by taking account of $q_0(n) = P_0 + \Delta q_0(n)$ and $P_0 \gg |\Delta q_0(n)|$, Q is given as

$$\begin{aligned} Q &= q_1^2 - \langle q_1^2 \rangle \simeq q_1^2 - \langle q_1 \rangle^2 \\ &\simeq \left(j \frac{kS}{2\pi z N} \right)^2 \sum_{n=1}^N \sum_{m=1}^N [P_0 \{ \Delta q_0(n) + \Delta q_0(m) \}] \exp \left[-j \frac{k}{2} \frac{(x-x_n)^2 + (y-y_n)^2 + (x-x_m)^2 + (y-y_m)^2}{z} \right] \\ &= \left(j \frac{kS}{2\pi z N} \right)^2 P_0 \sum_{n=1}^N \exp \left[-j \frac{k}{2} \frac{(x-x_n)^2 + (y-y_n)^2}{z} \right] \sum_{m=1}^N 2\Delta q_0(m) \exp \left[-j \frac{k}{2} \frac{(x-x_m)^2 + (y-y_m)^2}{z} \right]. \end{aligned} \quad (21)$$

The summation term with respect to n denotes the sound field subject to uniform pressure distribution with P_0 , whereas the summation term with respect to m denotes the variation in pressure q_1 around its mean value $\langle q_1 \rangle$. As stated previously in the linear field evaluation, the variance of the latter term in m is approximately independent of the variables x and y . Since the source term Q of Eq. (20) is formed by the product of the above two terms, it may be expected that the range dependence of the standard deviation $\sigma_2 = \sqrt{\langle \Delta q_2 \Delta q_2^* \rangle}$ along the x - and/or y -axis does not change greatly compared with that of the mean value of the fundamental component.

In the same way as the linear field case, we can obtain the coefficient of variation CV_2 for the second harmonic component. From Eq. (21), the deviation σ_2 is proportional to $\sqrt{\langle QQ^* \rangle}$, then to $P_0 \times 2\sigma$. In addition, the magnitude of the mean $\langle q_2 \rangle$ is obtained by replacing $2\Delta q_0(m)$ with P_0 in summation m . Thus, the average of the second harmonic is related to P_0^2 and the standard deviation is related to $P_0 \times 2\sigma$. CV_2 is then expected to be as follows:

$$CV_2 = \frac{\sigma_2}{|\langle q_2 \rangle|} = 2 \frac{\sigma}{P_0 \sqrt{N}}. \quad (22)$$

The coefficient of variation for the second harmonic is twice as large as that of the fundamental component.

3. NUMERICAL IMPLEMENTATION

In order to verify the effectiveness of the present theoretical prediction, we perform numerical verification using a computer simulation technique. The approach uses the Monte Carlo method.

Figure 2 shows a theoretical model of an array sound source, the aperture of which is a rectangle of length $2a$ in the x direction and of length $2b$ in the y direction. The area of the aperture is then $4ab$, being divided into N equal subareas. These subareas are numbered sequentially from #1 to # N , as shown in Fig. 2. We assume that the array

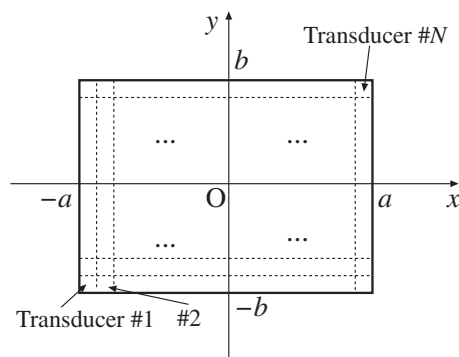


Fig. 2 Array source model for computer simulation. The array consists of N small transducers, the apertures of which are all equal to S/N , where S is the aperture area of the array and is equal to $4ab$.

source with pressure amplitude $P_0 = 50$ Pa (which corresponds to approximately 125 dB in SPL) is radiating 30 kHz ultrasonic waves in air. Specifically, the aperture dimensions are assigned as $a = 10$ cm and $b = 8$ cm. Simulation is performed for two transducers of different size: (i) 1 cm \times 1 cm and (ii) 2 cm \times 2 cm. Both transducers will exhibit almost omni-directional patterns because the dimensions are comparable with the wavelength of 1.1 cm. For each arrangement, the number N takes a value of 320 for (i) and 80 for (ii). The air temperature and relative humidity of meteorological factors under normal conditions are chosen as 20°C and 50%, respectively. Both factors realistically influence sound absorption, although not considered in the theory in the preceding section. The absorption coefficients at 30, 60, and 90 kHz are predicted to be 0.108, 0.228, and 0.338 Np/m, respectively [12].

The flowchart of computational procedure is shown in Fig. 3. First, 80 and 320 pseudo-random numbers that obey Gaussian distributions with a mean value of 27.6 and a standard deviation of 4.54 are generated numerically as input data [13]. The random numbers are then multiplied by 1.81 (= 50/27.6) so that the mean pressure amplitude on the source face P_0 may become 50 Pa. Next, the numbers thus obtained are sequentially allocated as the pressure amplitudes of the individual transducers. Numerical analysis to solve the KZK equation is based on the alternating direction implicit (ADI) scheme used in finite difference methods that are usually employed in three dimensional wave propagation problems [7]. The first seven harmonics are retained in the computation on the condition that the initial step sizes in the x and y directions are both 2.5 mm and the initial size in the z direction is 2.2 mm [14]. During propagation, all of the step sizes are gradually increased

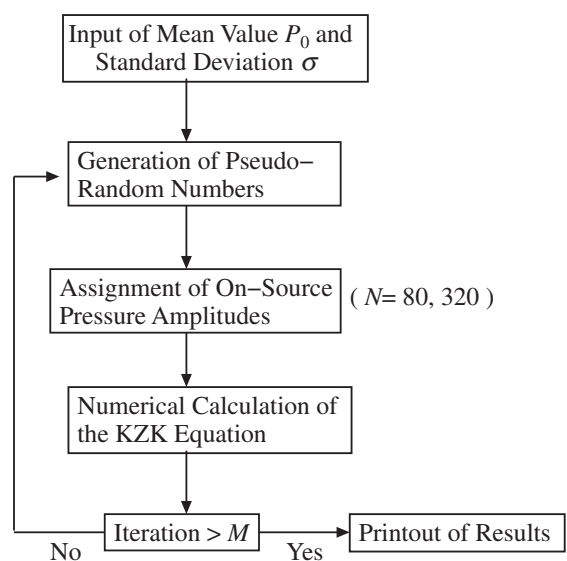


Fig. 3 Flowchart of the simulation. The number of trials, M , in calculation is 100.

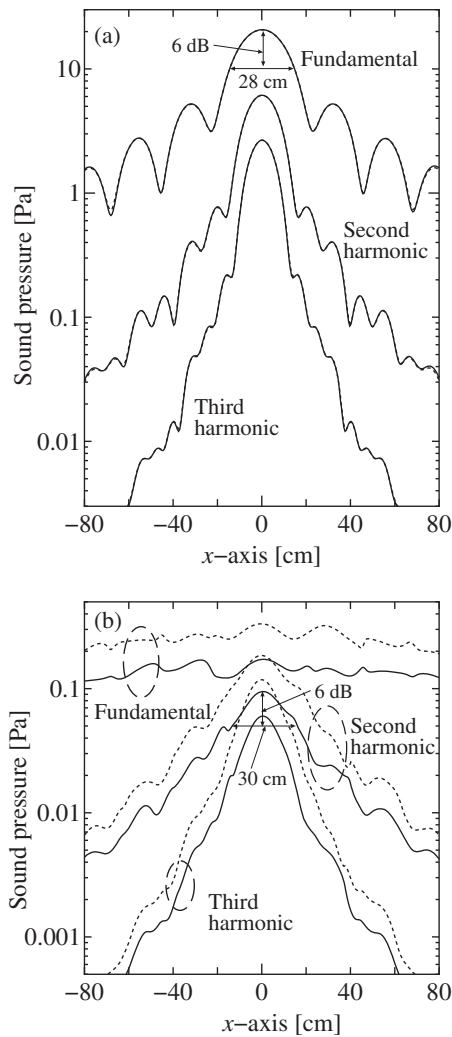


Fig. 4 Range-dependent mean values (a) and standard deviations (b) for the first three harmonics of sound pressures along the x -axis at $z = 4$ m. Solid curves denote the data for $N = 320$, and dotted curves denote the data for $N = 80$. The curves of the mean pressures almost overlap for $N = 80$ and 320 .

subject to the transformation rule of the coordinates [15]. A similar computation is repeated 100 times while changing the initial random numbers and retaining the same mean and standard deviation.

Figure 4 shows the range-dependent curves of the first three harmonic pressures along the x -axis at $z = 4$ m, in which (a) indicates the mean amplitudes and (b) indicates the standard deviations. Numerical data along the y -axis are not shown because their characteristic tendencies are similar to those along the x -axis. In both figures, the solid and dotted curves denote the data for $N = 320$ and $N = 80$, respectively.

As Eq. (8) predicts, the pressure amplitudes are not discernible even when the number of transducers is changed from $N = 80$ to 320 , i.e., the solid and dotted lines entirely overlap within the range of ± 80 cm. More-

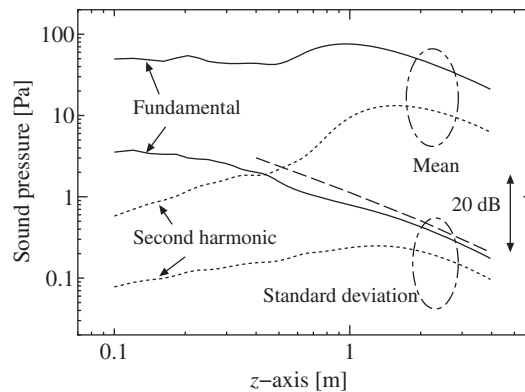


Fig. 5 Mean pressure amplitudes and standard deviations of the fundamental and second harmonic beams along the z -axis when $N = 320$. The dashed line denotes the theoretical curve predicted from Eq. (12).

over, the curves are symmetric with respect to the central axis of $x = 0$. On the other hand, remarkable differences appear in the data for the standard deviations. For example, the pressure amplitudes increase in inverse proportion to \sqrt{N} , as Eq. (12) predicts, i.e., when $N = 80$, sound pressures are approximately twice, or 6 dB ($= \sqrt{320/80} = 2$), greater in comparison with $N = 320$. This tendency of 6-dB difference can be observed for the three harmonics even in the region away from the beam axis. Interestingly, the standard deviations of the fundamental component are almost independent of the coordinate variable x . However, those of the higher harmonics are distinctly dependent on x so as to decrease with the distance from the beam axis. Incidentally, the -6 dB width of the second-harmonic standard deviation is 30 cm when $N = 320$, so that the width is almost the same as that of the mean value of the fundamental component, i.e., 28 cm. This result is expected from the discussion in Sect. 2.2.

The coefficient of variation CV_1 in the farfield for the fundamental beam is predicted to be $4.54/(27.6 \times \sqrt{320}) = 9.2 \times 10^{-3}$ by Eq. (15) when $N = 320$. Based on the data presented in Fig. 4, the simulation indicates that CV_1 is approximately 9×10^{-3} because the mean pressure is 20 Pa and the standard deviation is 0.18 Pa, which is in approximate agreement with the theoretical result. Similarly, CV_2 for the second harmonic takes a value of 0.018 from Eq. (22) and is approximately the same as the value 0.016 obtained from simulation in Fig. 4 (the mean pressure of q_2 is 6.0 Pa and the standard deviation is 0.093). It then follows that CV_2 is approximately 6 dB higher than CV_1 , as Eq. (22) predicts.

Propagation curves are shown in Fig. 5 for the mean pressure amplitudes and standard deviations of the fundamental and second harmonic beams. The mean amplitudes of the fundamental beam maintain an approximately constant magnitude up to 1 m from the source and then

decay gradually with the propagation distance. The decay curve is roughly -6 dB/dd , primarily due to spherical spreading. Similarly, the standard deviation decays in parallel with the -6 dB/dd line predicted by Eq. (12). In reality, the decay curve is corrected by multiplying the amplitude attenuation factor $e^{-\alpha_1 z}$, where α_1 is the absorption coefficient of the fundamental wave at 30 kHz and is given by $\alpha_1 = 0.108\text{ Np/m}$. We can then expect that simulation asymptotically approaches the theoretical curve in the farfield.

The level difference between the mean pressure and standard deviation at 4 m is approximately 40 dB. However, the difference becomes small near the source. For example, the difference is almost halved, being less than 20 dB within the range of 0.2 m. This means that the variation in performance of individual transducers plays a more significant role in the nearfield than in the farfield. Although the same is observed for the second harmonic curves, both the mean and standard deviation tend to increase with propagation up to 1.5 m, which differs from the pressure curves of the fundamental beam.

3.1. Comparison with Experiment

Kawashima *et al.* reported experimental data on CVs for the fundamental and second harmonic pressure waves using a square aperture array source with with $16\text{ cm} \times 16\text{ cm}$ that is composed of 256 piezoelectric ceramic transducers with a resonance frequency of 40 kHz and an aperture diameter of 10 mm. The CV of the transducers was set to be 30%. The experimental procedure and data acquisition are described in detail in their technical report [6].

Figure 6 shows the experimental and simulation data for the CVs of sound pressure. The data for two cases are presented: (a) the data along the z -axis and (b) the data along x -axis at $z = 1\text{ m}$. Solid lines and symbols denote simulated results and measurement data, respectively. In (a), the CV curves take a peak at 45 cm for the fundamental and at 60 cm for the second harmonic, respectively. These peaks are expected to be located at the dips of the mean values of sound pressure [14]. Actually, the last dips of the fundamental component and second harmonic are theoretically located at $0.16 \times R_0$ and $0.21 \times R_0$, respectively. In these predictors, R_0 is the Rayleigh length ($= S/\lambda$, where λ is the wavelength) [14]. Since $S = 256\text{ cm}^2$ and $\lambda = 8.6\text{ mm}$, the peak of the fundamental component, for example, should appear at 47 cm, which is almost equal to the data in Fig. 6(a). In the region far from the peaks, the CV values decrease gradually with distance, approaching the values predicted by Eqs. (15) and (22), as indicated by the dotted lines. In addition, CV increases with the radial distance, as shown in Fig. 6(b). Roughly, the agreement between the simulation and experimental results is good in the region more than 80 cm from the array source and within 10 cm

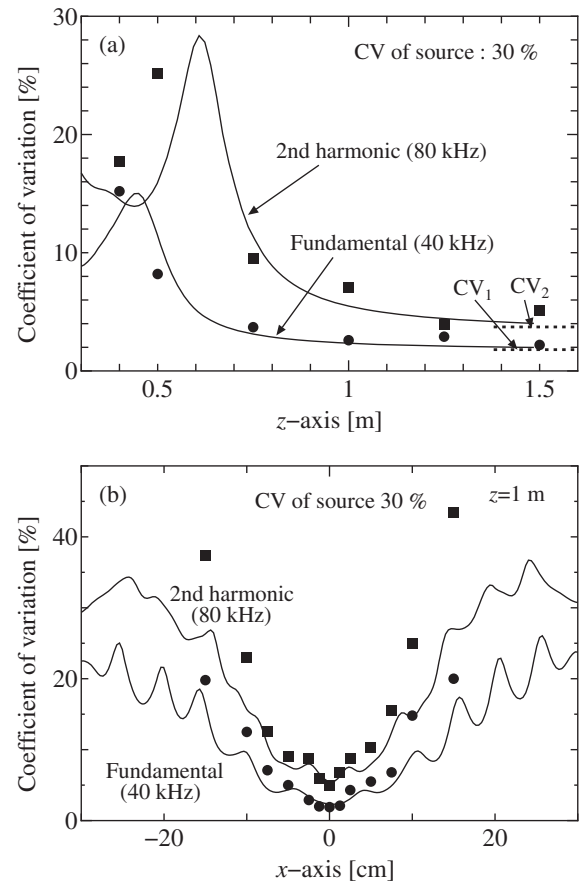


Fig. 6 Coefficients of variation of the fundamental and second harmonic components (a) along the z -axis and (b) along the x -axis at $z = 1\text{ m}$. The CV of the ultrasonic transducers is 30%. The solid lines denote the simulated curves, and the symbols denote the measurement data. The dotted lines in (a) are predicted from Eqs. (15) and (22).

of the z -axis. Except for these regions, however, relatively significant discrepancies appear. A possible source for the discrepancies is the neglecting of the phase variation of the transducers. The aperture of the transducer is a square in the simulation, but is circular in the experiment. This might be another source of the discrepancies.

4. CONCLUSIONS

In general, piezoelectric ultrasonic transducers have more or less variation in their performances or conversion efficiencies in a random manner. Under such assumption, we considered the effect of the variation on sound field formation from a statistical point when an array source consisting of a number of transducers with such variations radiates monochromatic waves of finite amplitude. The theory predicts that random variation in pressure amplitude decreases with the increase in the number of transducers N . More strictly, the standard deviation of pressure amplitude is inversely proportional to \sqrt{N} . One of the interesting findings is that the pressure variation decreases as the

pressure receiver is moved away from the array source. These findings are effective for both the fundamental and second harmonic components. However, a significant difference appears in the beam pattern curves of the standard deviation. In a linear field, the pattern is approximately independent of the radial coordinate. Whereas, the pattern is obviously dependent on the coordinates, being almost the same pattern of the mean value of the fundamental component. The validity of the present findings was verified through a Monte Carlo computer simulation and/or experiments conducted in air.

ACKNOWLEDGMENTS

The present study was supported in part by Grant-in-Aid for Scientific Research (B) No. 22360094 from the Japan Society for the Promotion of Science and by the Regional Innovation Strategy Support Program 2013 from the Ministry of Education, Culture, Sports, Science and Technology.

REFERENCES

- [1] H. Kwun, W. D. Jolly, G. M. Light and E. Wheeler, "Effects of variations in design parameters of ultrasonic transducers on performance characteristics," *Ultrasonics*, **26**, 65–72 (1988).
- [2] S.-C. Wooh and Y. Shi, "Influence of phased array element size on beam steering behavior," *Ultrasonics*, **36**, 737–749 (1998).
- [3] F. J. Pompei and S.-C. Wooh, "Phased array element shapes for suppressing grating lobes," *J. Acoust. Soc. Am.*, **111**, 2040–2048 (2002).
- [4] S. A. Goss, L. A. Frizzell, J. T. Kouzmanoff, J. M. Barich and J. M. Yang, "Sparse random ultrasound phased array for focal surgery," *IEEE Trans. Ultrason. Ferroelectr. Freq. Control*, **43**, 1111–1121 (1996).
- [5] X. Ji, J.-F. Bai, G.-F. Shen and Y.-Z. Chen, "High-intensity focused ultrasound with large scale spherical phased array for the ablation of deep tumors," *J. Zhejiang Univ. Sci. B*, **10**, 639–647 (2009).
- [6] H. Kawashima, K. Aoki and T. Kamakura, "Effect of a variation in source pressure distribution on nonlinear sound field," *Tech. Rep. IEICE*, **US98-97**, 1999 (in Japanese).
- [7] S. Saito and T. Kamakura, "Nonlinear propagation of sound waves," in *Nonlinear Acoustics: Fundamentals and Applications*, T. Kamakura, Ed. (Corona Publishing, Tokyo, 2014), Chap. 2 (in Japanese).
- [8] T. Kamakura, M. Tani, Y. Kumamoto and K. Ueda, "Harmonic generation in finite amplitude sound beams from a rectangular aperture source," *J. Acoust. Soc. Am.*, **91**, 3144–3151 (1992).
- [9] H. Lee, J. Tak, W. Moon and G. Lim, "Effects of mutual impedance on the radiation characteristics of transducer arrays," *J. Acoust. Soc. Am.*, **115**, 666–679 (2004).
- [10] Y. Wada, "Nonlinear propagation of sound beams from a rectangular aperture source," Master thesis of Electronic Engineering, The University of Electro-Communications (1995.2) (in Japanese).

- [11] W. B. Davenport and W. L. Root, *An Introduction to the Theory of Random Signals and Noise* (McGraw-Hill, New York, 1958), Chap. 5.
- [12] H. E. Bass, L. C. Sutherland, J. Piercy and L. Evans, "Absorption of sound," in *Physical Acoustics*, W. P. Mason and R. N. Thurston, Eds. (Academic, New York, 1984), Vol. XVII.
- [13] Y. Ono and K. Isoda, Eds., *Handbook for Numerical Calculation* (Ohmsha, Tokyo, 1990), Chap. 16 (in Japanese).
- [14] T. Tsuchiya and T. Kamakura, "Numerical simulation for nonlinear fields," in *Nonlinear Acoustics: Fundamentals and Applications*, T. Kamakura, Ed. (Corona Publishing, Tokyo, 2014), Chap. 4 (in Japanese).
- [15] M. F. Hamilton, J. N. Tjøtta and S. Tjøtta, "Nonlinear effects in the farfield of a directive sound source," *J. Acoust. Soc. Am.*, **78**, 202–216 (1985).

APPENDIX A: PROBABILITY DENSITY FUNCTION OF PHASE

Ultrasonic waves emitted from the source are composed of a collection of harmonically related sinusoidal signals that are generally given by $s(\theta) = P_0 \sin \theta$, where θ is the phase. In order to know how the only phase affects field formation, we assume the amplitude P_0 to be constant, whereas the phase θ is assumed to be a random variable that obeys a Gaussian distribution of the form

$$p(\theta) = \frac{1}{\sqrt{2\pi}\sigma_\theta} e^{-\theta^2/2\sigma_\theta^2}, \quad (\text{A-1})$$

where the notation p is not the sound pressure, but rather the probability density function with small standard deviation σ_θ . Thus, the sinusoidal function $s(\theta)$ can be viewed as a stochastic process and its probability function $p(s)$ is obtained as

$$\begin{aligned} p(s) &= p(\theta) \frac{1}{ds/d\theta} = p(\theta) \frac{1}{P_0 \cos \theta} \\ &= \frac{1}{\sqrt{2\pi}\sigma_\theta} \frac{1}{\sqrt{P_0^2 - s^2}} e^{-\{\sin^{-1}(s/P_0)\}^2/2\sigma_\theta^2}. \end{aligned} \quad (\text{A-2})$$

Actually, σ_θ in Eq. (A-1) is evaluated as small as 0.1 radians, according to the measured data in Fig. 1. Hence, Eq. (A-2) can be approximated as

$$p(s) \simeq \frac{1}{\sqrt{2\pi}\sigma_\theta P_0} e^{-s^2/2\sigma_\theta^2 P_0^2}. \quad (\text{A-3})$$

Note that the random change in phase affects the formation of the pressure field as $\sigma_\theta P_0$, corresponding to the effect due to the random change of the amplitude only, namely, σ_{P_0} . Since $\sigma_\theta P_0 = 0.1 \times 27.6 = 2.76$ Pa and $\sigma_{P_0} = 4.54$ Pa from Fig. 1, it can be predicted that in the numerical examples of Figs. 4 and 5 the amplitude effects are 1.6 times greater than the phase effects.